CHAPTER 3

Development and Optimization of Methotrexate Chitosan Nanocarrier for Breast Cancer Treatment

3.1 Introduction

Breast cancer is the primary reason for cancer-related deaths in women worldwide, and its incidence is rising yearly [174]. The three primary cancer treatment modalities are chemotherapy, radiation therapy, and surgery [175]. However, the significant issues are the drawback of the current therapies, such as poor drug selectivity for tumor cells or non-specific toxicity against the normal cell, insufficient drug concentration in tumor cells, and severe side effects [176]. The most effective drug delivery to the intended site of action in the body is required for optimal pharmacological action. Remarkable efforts have been made to develop therapeutics for site-specific drug delivery [177]. Nano-scaled drug delivery system (NDDS) has been recognized as one of the most promising ways to treat cancer via the enhanced permeability and retention (EPR) effect. Nanotechnology has emerged as a potentially helpful technique for administering various cytotoxic drugs and can be effectively used to minimalize formulation-related toxicities [178,179]. In recent years, a more profound comprehension of tumor biology and greater accessibility to flexible materials, such as polymers [180], lipids [181], inorganic carriers [182], and polymeric hydrogel, has been identified [183]. Polymeric nanocarriers (PNCs) have become reliable drug delivery carriers because they can encapsulate different drugs and recognition elements for cargo delivery at the desired locations [184,185]. They successfully serve as a drug delivery system to enhance the anticancer properties of numerous drugs. It has been observed that the anticancer drug-loaded polymeric

nanoparticles accumulated more in the tumor tissues than in normal tissues. The leaky nature of the tumor vasculature promotes the accumulation of nanoparticles in the tumor cells through the EPR effect [186].

The delivery of a drug via a nanoparticle approach may be one way to achieve this goal due to its small size. It may be helpful to the controlled release of a drug at a target site for prolonged therapeutic activity. Many polymeric nanocarriers, including poly (lactic-co-glycolic-acid) (PLGA) nanoparticles [187], poly (hydroxyl alkanoates) (PHAs) [188], poly (3-hydroxybutyrate) (PHB) base nanoparticles [189] and chitosan-based nanoparticles [190,191]. Either passively or actively targeting malignant cells was employed in various fields. This would minimize side effects while enhancing therapeutic efficacy because of their superior biocompatibility [192], simple cross-linking [193], controllable drug release [194], and stimulus-triggered release [195]. Here Methotrexate (MTX) is used as a model drug in this study. It is an anti-folate drug and competitive inhibitor of dihydrofolate reductase [196]. It is frequently used as a chemotherapeutic drug to treat human malignancies [197], such as solid tumors [13], breast cancer, lymphomas, and colon cancer [19]. However, due to its non-specific drug delivery, MTX has been reported to have harmful side effects such as neurotoxicity and other associated toxicities to healthy cells. Therefore, reducing its side effects by increasing therapeutic efficacy [23], chitosan is used as a carrier to deliver MTX. Chitosan (CS) is a naturally occurring linear polysaccharide [42] that is produced from partially deacetylated chitin. It comprises β-(1-4) linked D-glucosamine and N-acetyl-D-glucosamine units, randomly distributed [56] in the chain. It is the most preferred biopolymer due to excellent biocompatibility [198,199], biodegradability [200], and surface functionalization ability [41].

3.2 Experiment Section

3.2.1 Preparation of MTX-encapsulated chitosan nanocarrier

Methotrexate-encapsulated chitosan nanocarriers (M-CNCs) were synthesized per the reported method with some modifications [201]. The Taguchi design (DOE) has been implemented to improve the quality of the preparation process. An aqueous chitosan stock solution (0.5 mg/ml) was freshly made by dissolving it in a glacial acetic acid solution (1% v/v) and constantly stirring until a clear solution was achieved [202]. Then take 10 ml of the chitosan solution and adjust the pH to 4.6 by adding a 1N sodium hydroxide solution (NaOH) and 3 ml of tripolyphosphate (0.5 mg/ml) dropwise. Then 10 ml of Methotrexate solution (0.5 mg/ml) was added. The reaction continued for an hour with contentious stirring by a magnetic stirrer at 800 rpm at 37°C. The resulting nanoparticles were centrifuged at 15000 rpm for 20 minutes. The nanoparticles were then collected, rinsed 2-3 times with distilled water, dried in a vacuum oven overnight, and stored for characterization of M-CNCs.

3.2.2 Design of Experiments (DOE)

3.2.2a Taguchi orthogonal array design

It is known that a full factorial design is one in which all possible combinations of the various factors (independent variables) at different levels are studied. While factorial experimentation is instrumental and is based on strong statistical foundations, it becomes unmanageable in the usual industrial context. As the number of factors and their levels increases, the number of experiments becomes prohibitively large. And for conducting so many experiments, many batches of materials, different process conditions, etc., result in heterogeneity, and the experimental results must be more accurate (results in more experimental error). Taguchi significantly decreased the number of experiments required

to reach the optimum parameters. This is made possible by including the concept of orthogonal arrays in the design of experiments (DOE). Proper choice of independent variables minimizes the variation from the target value, and its product performance becomes insensitive to uncontrolled (noise) factors, enabling desired optimum output in a small number of trials. This approach has been applied in the area of administration, marketing, hospitals, pharmaceutical [203], food industry [204], energy, architecture [205,206], chromatography [207], and physical processes, as well as computer simulation models [208]. Integral to DOE is regression analysis, a popularly used statical tool. It provides functional relationships among various variables and is used to develop models to forecast optimum output from the measured variables. For instance, in the case of multiple regression, a series of data points are fit to a straight line, which relates one dependent variable to multiple independent variables.

Design of experiments is a methodical tool for optimizing formulation design by obtaining a suitable mathematical model with the fewest number of runs. Several critical quality attributes (CQAs). CQAs, such as hydrodynamic size (Z_{avg}), percent entrapment efficiency (% EE), and percent drug loading (% DL), were investigated during optimization. Several critical materials attributes (CMSs), such as the pH of chitosan solution and polymer/cross-linker ratio, and necessary processing parameters (CPP), such as reaction time, were considered to obtain their effects on the response variables. These independent variables have been studied at three different levels such as low (-), medium (0), and high (+), as shown in Table 3.1. Based on the preliminary experiments, select the low, medium, and high level of process variables parameters to optimize the nanocarrier properties per requirements.

Taguchi orthogonal array, a 3-level-3-factor, was applied using Minitab17 statistic software (Statistical Software Release, Version 17.3.1. Minitab Inc. USA). The design

consisted of 9 runs, as shown in Table 3.2**.** The Taguchi design was employed to minimize nanocarrier size (Y_1), maximize entrapment efficiency (Y_2), and drug loading (Y_3). Through the use of Analysis of Variance (ANOVA and multiple linear regressions, the impact of factors and their interactions on the response variables was investigated.

Table 3.1. *Selected factors at three different levels and the responses*

	Level			
Parameters	**Code**	**Low level (-)**	**Mid-level (0)**	**High level (+)**
X_1=pH (of the chitosan solution)	A	2.4	4.4	6.4
X_2=Polymer/cross-linker ratio (v/v)	B	10/1	10/3	10/5
X_3=Reaction Time (h)	C	1	3	6
Responses	**Goal**			
R_1= Nanocarrier size (Zavg) [a]	To minimize			
R_2=Percentage entrapment efficiency (EE)	To maximize			
R_3=Percentage drug loading (DL)	To maximize			

Table 3.2. *Taguchi design (DOE.) L9 (3 ^ 3) orthogonal array*

Factors (Independent variables)				**Response (Dependent variables)**		
Experimental Runs	**pH**	**P/CL Ratio (v/v)**	**RT (hr)**	**Zavg (Y_1) (nm)**	**EE (Y_2) (%)**	**DL (Y_3) (%)**
1	2.4	1	1	160±8.0	68	12
2	2.4	3	3	186± 6.3	74	34
3	2.4	5	6	200±7.2	72	12
4	4.4	1	3	634±8.8	50.6	52
5	4.4	3	6	224±6.9	58.2	44
6	4.4	5	1	102±7.5	60.4	42
7	6.4	1	6	494±6.6	63.7	56
8	6.4	3	1	216±6.8	99.2	36
9	6.4	5	3	352±5.9	77	56

P/CL ratio; Polymer/Cross-linker ratio, RT; Reaction Time (hr). Z_{avg}*; Average Particle size (Hydrodynamic size) (*Y_1*), EE (%); Percent Entrapment Efficiency (*Y_2*), DL (%) Percent Drug Loading (*Y_3*).*

3.2.2b Statistical optimization and data analysis

Based on Taguchi orthogonal array factorial design, nine batches performed in triplicate were analyzed using Minitab 17 software. The effect of 3-independent variables is the pH of the chitosan solution (2.4, 4.4 and 6.4), polymer/cross-linker ratio (10/1, 10/3, and 10/5 ml), and reaction time (1,3 and 6 hours) on 3-response variables; size, percent entrapment efficiency, and percent drug loading, analyzed by one-way analysis of variance (ANOVA) and by the signal-to-noise ratio. Signal-to-noise ratios quantified the variable design more significantly. For example, smaller is better for $\mathrm{S/N} = -10\log\left(\frac{1}{\mathrm{n}}\sum_{i=1}^{n}\mathrm{y2}\right)$, and larger is better for, $\mathrm{S/N} = -10\log\left(\frac{1}{n}\sum_{i=1}^{n}\frac{1}{y2}\right)$.

Whereas. $\bar{y}$ is average of observed data, s_y^2 is a variance of y, n is the number of observations, and y^2 is the observed data, and the higher the S/N ratio, the improved the outcome. ANOVA was used to validate the fitted model. Further data were assumed to be statistically significant for $P<0.05$ [209].

3.2.2c Data analysis and validation

The 3D graphs and contour plots describing the polynomial regression and optimized formulations were selected. Predicted responses were selected based on desirability factors. Criteria for optimal formulations were framed based on minimum particle size, maximum drug loading, and high entrapment efficiency. The optimal formulation served as a checkpoint to validate the RSM method, and polymeric nanocarriers were synthesized using these optimal process variables. The percentage errors were calculated according to values obtained for the responses and compared with estimated values. Finally, correlation graphs were plotted separately for each response. Furthermore, the numerical optimization was conducted by DOE using Minitab to identify the optimum

combination of constraints, justifying the desired conditions. This optimization aimed to get the maximum response that concurrently satisfied all variable properties.

3.2.3 Characterization

3.2.3a Physiochemical characterization

To investigate the possible chemical interaction between the drug, polymer, and M-CNCs by FTIR spectrometer (SHIMADZU, 8400S, Tokyo, Japan) using KBr method, and measurement was performed from 4000 cm to 400 cm^{-1} with a 4 cm^{-1} resolution with 20 numbers of a scan. The X-Ray Diffraction measurements were performed by an X-ray diffractometer (RIGAKU, Miniflex 600) within 2θ of 5° to 50° with a step size of 0.02°/step at a scan speed of 7°/min at 25°C. XRD was used to identify the phase present in Nanoparticles. The size and distribution of particles analyzed using HR-TEM were used to evaluate the morphology of the prepared nanoparticles. The measurements were performed on the HR-TEM model Tecnai G2 20 TWIN (FEI Company of USA). The TGA measurements were performed TGA-50 (Shimadzu Pte Ltd) in nitrogen gas with a flow rate of 20.0 ml/min within the temperature range from 30°C to 700°C at a heating rate of 10°C/min. The particle size and zeta potential (Zp) Nanoparticles have been measured using dynamic light scattering (DLS) (Malvern Zetasizer Nano ZSP, UK). The Z_{avg} was analyzed at 25°C using a polystyrene disposable cuvette at a backscatter angle of 173°, and the Zeta potential was measured using a universal dip cell (ZEN1002). The amount of un-entrapped drug in the supernatant was analyzed by UV-vis spectrophotometer (Eppendorf Biospectrometer kinetic) at 303 nm. The drug loading capacity (% DL) and percent entrapment efficiency (% EE) were calculated by using the following equation (Eq.3.1 & 3.2).

$$D\,L\,(\%) = \frac{Weight\ of\ the\ drug\ in\ the\ nanocarrier}{Weight\ of\ the\ nanocarrier} \times 100 \qquad Eq.3.1$$

$$EE\,(\%) = \frac{Weight\ of\ the\ drug\ in\ the\ nanocarrier}{Weight\ of\ the\ feeding\ drug} \times 100 \qquad Eq.3.2$$

3.2.3b Stability studies

The M-CNCs were kept in a tightly sealed glass vial, and the stability was checked at three sets of storage conditions, such as long-term stability for up to 90 days (at 4°C and 40°C), after three cycles of heating-cooling (40°C and 4°C), and after three cycles of freeze-thaw (-20°C and 25°C). Various stability-indicating parameters like organoleptic, physicochemical, and colloidal properties (Z_{avg}, PDI, and Zp) were evaluated at definite intervals during and at the end of the stability study.

3.2.4 *In-vitro* drug release

A dialysis membrane has been used to study the release of methotrexate from nanocarrier (Dialysis Membrane-135, cut off 12 kDa, Himedia, India) nanocarrier. The membrane was immersed in phosphate buffer solutions (PBS) with pHs of 6.4 and 7.4 overnight for activation. The formulation was placed in the dialysis bag, then knotted on both sides, suspended in 100 ml PBS and stirred at 50 rpm (37 ± 2°C). The aliquots (2 mL) were withdrawn at intervals of 0.08, 0.16, 0.25, 0.5, 0.75, 1, 2, 4, 6, 8, 10, 12, 24, 36, 48, 60, and 72 hours, then volume replenished with fresh PBS to maintain the sink condition. The sample was examined using a UV-Visible spectrophotometer at 303 nm. The experiment was conducted in triplicates, and results were expressed in average cumulative drug release (%) ± standard deviation using equation (Eq.3).

$$\% \, Cumulative \, release = \frac{Wt}{Wi} \times 100 \qquad Eq. 3.3$$

Whereas w_t is the amount of drug released at the time t, and w_i is the initial amount of the drug encapsulated in the nanocarrier. The amount of drug released was measured by a UV-Visible spectrophotometer at 303 nm.

3.2.5 Animal and treatment protocol

The animal ethical committee approval was taken from the Central Animal Ethical Committee, Faculty of Medicine, and Institute of Medical Science, Banaras Hindu University, dated 06/03/2021 (Protocol number. Dean/ 2021/IAEC/2544). All experiments involving animals comply with the ethical standards of animal handling. A female Sprague Dawley rat weight of 200±20 g was used for this study. The animal was obtained from the animal house of Indian Medical Science, Banaras Hindu University. Animals were maintained in a central animal facility at the Department of Pharmaceutical Engineering and Technology, IIT (BHU), acclimated at 25°C and 50% humidity under natural light/dark conditions provided with standard food and water ad libitum for one week before the experiment.

3.2.5.1 *In-vivo* pharmacokinetic studies

Free MTX and M-CNCs were administered intravenously to rats via the tail vein at a 5 mg/kg dose. Blood was collected from the retro-orbital plexus into EDTA-coated tubes at various intervals (0.25, 0.5, 0.75, 1, 2, 4, 8, 12, 24, 36, 48, and 72 hr). Plasma was isolated by centrifugation at 12000 rpm for 10 minutes at 4°C. The supernatant was withdrawn, and 20 µL plasma samples were used to quantify MTX by High-performance liquid chromatography (HPLC) analysis using the calibration curve of MTX in plasma.

The plasma was stored at -80°C until further use. The plasma drug concentration was plotted against time. Pharmacokinetic parameters (PK),

such as maximum plasma concentration (C_{max}), time until C_{max} is reached (T_{max}), plasma half-life ($t_{1/2}$), volume of distribution (Vd), area under the concentration-time curve (AUC), and plasma clearance (CL) was calculated using the Kinetica software (version 5.0, Thermo Fisher Scientific, Waltham, MA, USA).

3.2.5.1a High-performance liquid chromatography (HPLC)

A graded standard working solution was prepared by diluting the stock solution (10 µg/ml) into a concentration of 0.2, 0.4, 0.6, 0.8, and 1 µg/ml. HPLC, equipped with a C-18 column at 30 °C (4.6 mm ×250 mm ×5µm), was used for the analysis of Methotrexate at a wavelength of 303 nm [210]. Methanol and water were used as the mobile phase at a ratio of 70:30 v/v with a flow rate of 1 ml/minute. A calibration curve was prepared within the concentration range of 0.2–1 µg/ml by plotting concentration v/s in the area of the curve. Blood samples were collected from the rat retro-orbital plexus at given time intervals, and then whole blood was centrifuged at 10,000 × g for 10 minutes at 4°C to separate plasma. Then plasma was extracted with acetonitrile to remove extra protein and vortex for 5 minutes. After that, samples were centrifuged at 10,000 × g for 10 minutes, and then the supernatant was taken and dried. Then the dried powder was reconstituted in methanol and made at a different dilution of 0.1 to 1 µg/ml. The concentration of MTX in plasma was calculated by using the calibration curve.

3.2.6 Toxicity studies and histopathological examinations

The animals were divided into two treatment groups (three rats in each group); Group I: The normal control group (only saline), and Group II: received M-CNCs at an equivalent MTX dose of 5 mg/kg body weight through the tail vein. Blood was drawn from the retro-

orbital sinus in EDTA-coated tubes at intervals of 0.25, 0.5, 0.75, 1, 2, 4, 8, 12, 24, 36, 48, and 72 hours. Rats were sacrificed on days 7, 14, and 28 of the experiment to isolate the liver and kidneys. The collected tissue was immediately placed in a 10 % formalin solution for histology examinations. After fixation, tissues were cleaned in a graduated alcohol series, rinsed in xylene, embedded in paraffin, segmented using a microtome (5 μm thin), and stained with H & E stain. A standard optical microscope (Magnus MLX Plus microscope, Noida, Uttar Pradesh, India) was used at 10X magnification to examine any pathological alterations and abnormalities.

3.3 Characterization and Property Evaluation

3.3.1 Validation of the statistical model

3.3.1a Normal probability plots

Normal probability graphs were plotted between the residuals versus their estimated value and are shown in Figure 3.1**.** The residuals differ between the observed and the fitted response and should be typically scattered. The expected residual pH, polymer/cross-linker (P/CL) ratio, and reaction time (RT) for size (Y_1) are shown in Figure 3.1A and display somewhat close data points around the straight line representing customarily distributed data. Similarly**,** Figure 3.1B and Figure 3.1C display residual pH, P/CL ratio, and RT for percent entrapment efficiency (Y_2) and percent drug loading (Y_3), confirming linearly-fit data points. Hence, dependent variables seem to vary linearly with independent variables. All the data points lie within the range, showing that the experiments were carried out randomly, eliminating the chance of errors and confirming a good fit.

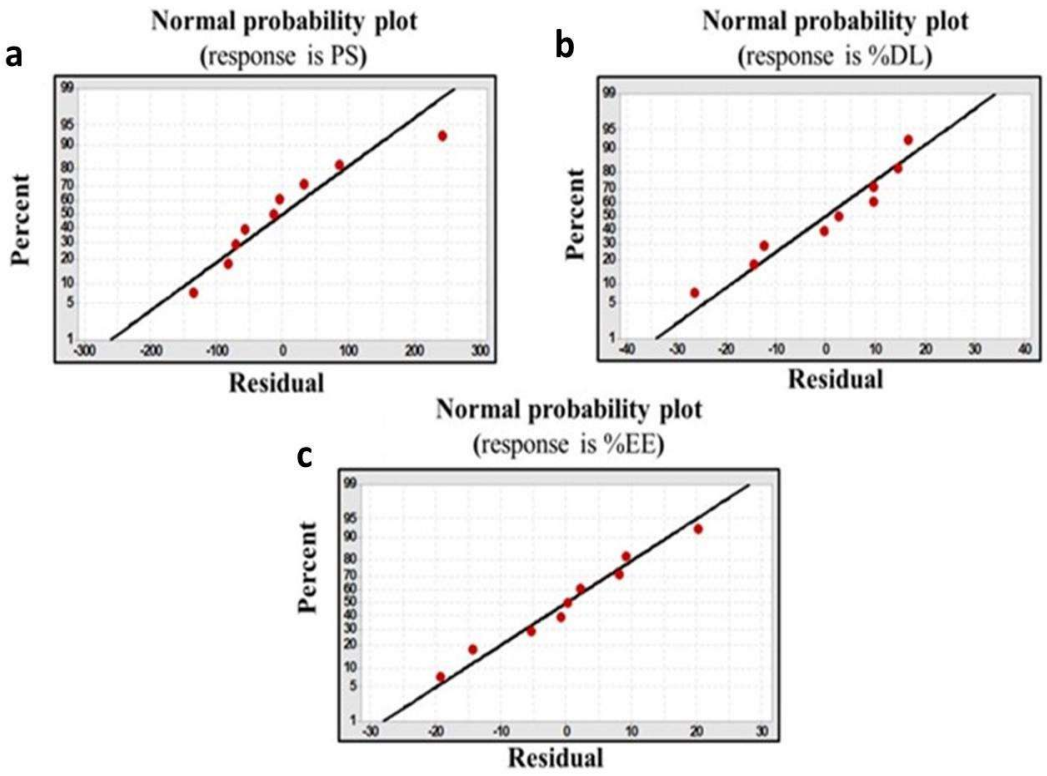

***Figure 3.1**: Normal probability plot A) Particle size, B) Entrapment Efficiency, and C) % drug loading.*

Nine runs performed in triplicate were analyzed using Minitab17 software based on Taguchi factorial design. The influence factor such as; pH (chitosan solution), polymer/cross-linker ratio, reaction time on responses, nanocarrier size, entrapment efficiency, and drug loading were analyzed by one-way analysis of variance (ANOVA). ANOVA was used to validate the fitted model. Further data were assumed to be statistically significant for $p < 0.05$.

According to ANOVA, Table 3.3 shows the nanocarrier size. The model p-value was 0.32, and the model terms (A, B, C, AA, BB, CC) have p-values above 0.05. The model R^2 value was found to be 87.93%. The higher value of R^2 reflects the ability of the chosen model to analyze and predict the results accurately.

Table 3.3. *ANOVA for Nanocarrier Size (Y_1)*

Analysis of variance					
Source	DF	Adj SS	Adj MS	F- Value	P- value
Model	6	215064	35844	2.43	0.032*
Linear	3	122748	40916	2.77	0.276
A	1	47883	47882.7	3.24	0.214
B	1	19953	19952.7	1.35	0.365
C	1	54913	54912.7	3.72	0.194
Square	3	92316	30772	2.08	0.341
A*A	1	968	968	0.07	0.822
B*B	1	22898	22898	1.55	0.339
C*C	1	68450	68450	4.64	0.164
Error	2	29528	14764		
Total	8	244592			
R-sq. 87.93%		R-sq(adj) 51.71%	R-sq(pred) 0.00%		

**P<0.05= (significant), **P< 0.01 (very significant), ***P<0.001(highly significant*

The ANOVA results of % EE are shown in Table 3.4. The model p-value (0.005) was below 0.05, and all the model terms (A, B, C, AA, BB, CC) have p-values below 0.05. The predicted R^2, adjusted $R^{2,}$ and signal-to-noise (S/N) represent the suitability of the statistical model for the response surface analysis and optimization. The model R^2 value was found to be 99.83%. The higher value of R^2 reflects the ability of the chosen model to analyze and predict the results accurately.

The ANOVA results of % DL are shown in Table 3.5. The model p-value (0.008) was below 0.05, and all the model terms (A, B, AA, BB, CC) have p-values below 0.05. The predicted R^2, adjusted $R^{2,}$ and signal-to-noise (S/N) represent the suitability of the statistical model for the response surface analysis and optimization. The model R^2 value was found to be 99.83%. The higher value of R^2 reflects the ability of the chosen model to analyze and predict the results accurately.

Table 3.4. *ANOVA for % Entrapment Efficiency (Y_2).*

Analysis of variance					
Source	DF	AdjSS	Adi MS	F-value	P- value
Model	6	1595.33	265.889	199.42	0.005**
Linear	3	1221.83	407.278	305.46	0.003**
A	1	13.5	13.5	10.13	0.086
B	1	504.17	504.167	378.12	0.003**
C	1	704.17	704.167	528.12	0.002**
Square	3	373.5	124.5	93.37	0.011*
A*A	1	112.5	112.5	84.37	0.012*
B*B	1	40.5	40.5	30.37	0.031*
C*C	1	220.5	220.5	165.37	0.006*
Error	2	2.67	1.333		
Total	8	1598			
R-sq 99.83%	R-sq(adj) 99.33%	R-sq(pred) 96.62%			

**P<0.05= (significant), **P< 0.01 (very significant), ***P<0.001(highly significant)*

Table 3.5. *ANOVA for % Drug loading (Y_3).*

Analysis of variance					
Source	DF	Adj SS	Adi MS	F- value	P value
Model	6	6693.33	1115.56	119.52	0.008*
Linear	3	1373.33	457.78	49.05	0.02*
A	1	600	600	64.29	0.015*
B	1	770.67	770.67	82.57	0.012*
C	1	2.67	2.67	0.29	0.646
Square	3	5320	1773.33	190	0.005**
A*A	1	648	648	69.43	0.014*
B*B	1	3872	3872	414.86	0.002**
C*C	1	800	800	85.71	0.011*
Error	2	18.67	9.33		
Total	8	6712			
R-sq 99.72%	R-sq(adj) 98.89	R-sq(pred) 94.37%			

*P<0.05= (significant), **P< 0.01 (very significant), ***P<0.001(highly significant)

3.3.1b Main effect plot

The main effect plots for three responses found from Taguchi orthogonal array design are shown in Figure 3.2**.** The main effect is present when the mean response changes across the level of a factor. Furthermore, the S/N ratio for the complete set of experiments was also evaluated using one-way ANOVA. The S/N ratio provides insight into the parameters that contribute significantly to the variation in the dependent variables. For example, in the case of nanocarrier size, the S/N ratio is "smaller the better," and for drug loading and entrapment efficiency, "large the better" is considered. The effect of parameters at different levels was identified by comparing S/N ratios for each response, and these factors were ranked based on the delta value. The delta value signifies the more effective its parameter contributes. Therefore, the optimum conditions obtained by this approach are as follows; C3B1A3 for particle size, A3C1B2 for % entrapment efficiency, and A3B1C2 for % drug loading.

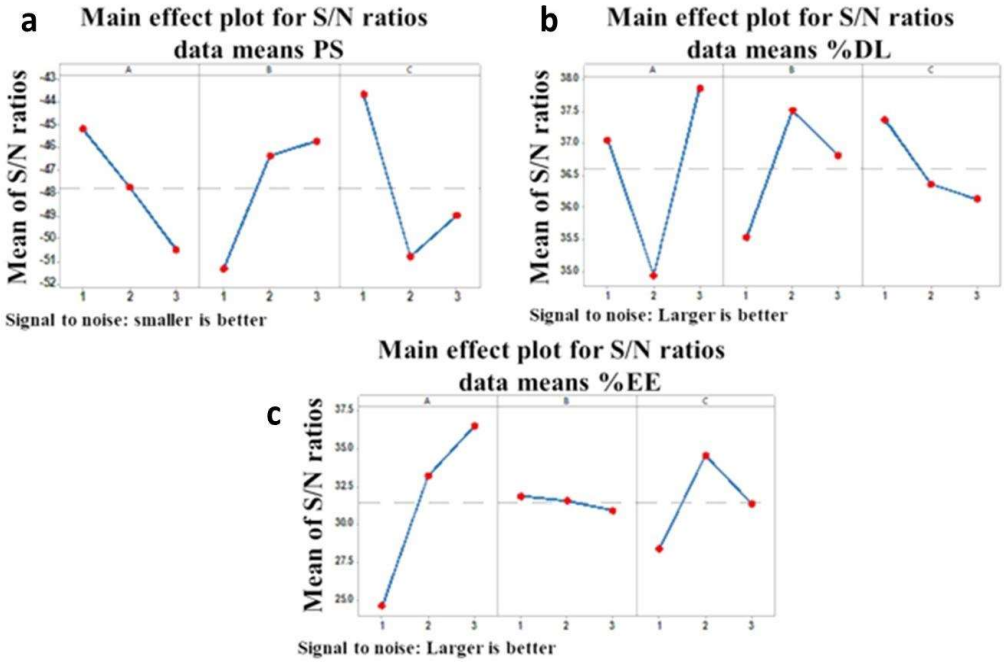

Figure 3.2: *S/N graph for Nanocarrier size (a), % Drug loading (b), and % Entrapment efficiency (c)*

3.3.2 Response surface analysis

The results of the effects of various factors on the chosen responses were presented in terms of response surface images (3D graphs and 2D contour) (Figures 3.3, 3.4 & 3.5) and regression equations (Eq.3.4, 3.5 & 3.6).

3.3.2a Influence of independent parameters on particles size

The influence of various factors on particle size is shown in Figure 3.3 and Eq 3.4. The obtained nanocarrier size ranges from 102 ± 29 to 634 ± 15 nm. On increasing the pH and polymer-to-cross-linker ratio, the size of the nanocarrier increases, which may be due to the cross-linking between chitosan and STPP. Further, by decreasing the reaction time, the particle size was found to be increased. Multiple linear regressions generate mathematical polynomial equations with constants and regression coefficients. Eq.3.4 can explain the effect of the independent parameter on particle size;

$$Y1 = 364 + 1X_1 + 370X_2 - 644X_3\ 22X_1^2\ 107X_2^2\ \ 185\ X_3^2 \qquad Eq.3.4$$

regression equations depicted the relationship of the variables to the measured response. The positive coefficient of the factor (independent variables) in the polynomial equation suggested a direct relationship with the response (dependent variables), whereas the negative coefficient indicated an inverse relationship. The pH and polymer-to-cross-linker ratio positively influence particle size, whereas the reaction time inversely affects the particle size. The higher the magnitude of the coefficient, the higher the contribution of that factor toward the selected response. The greater extent of the polymer-to-cross-linker ratio coefficient represents its highest contribution toward the particle size.

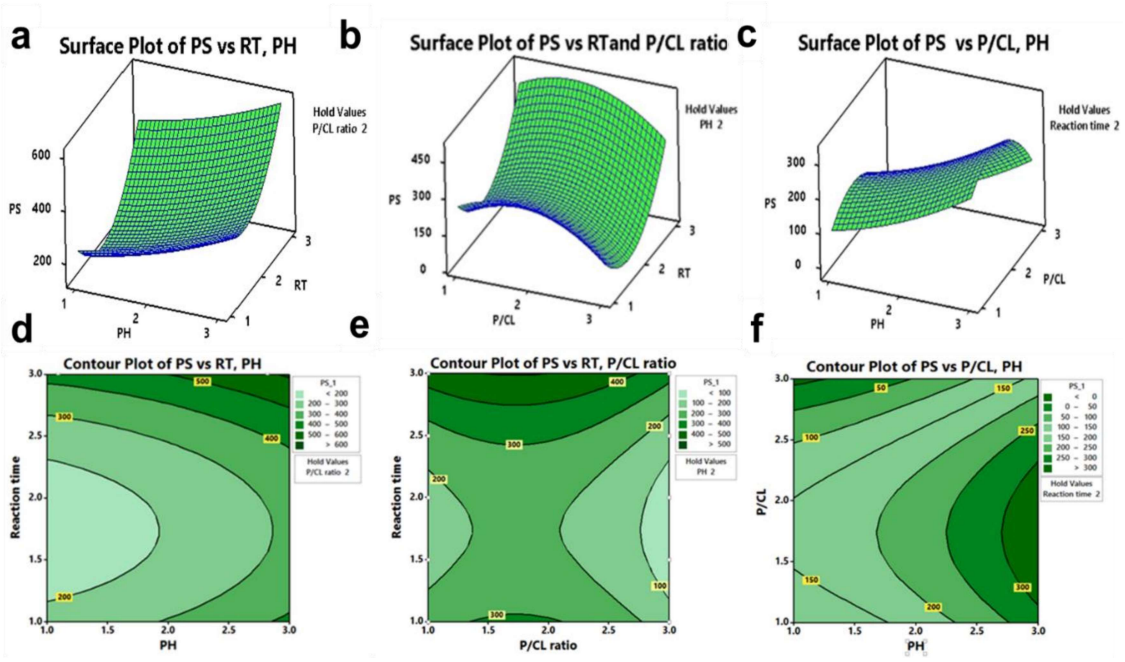

Figure 3.3: *3D response surface (a, b, & c) and their corresponding 2D contour plot (d, e, & f) showing mutual interaction and discrete effects of different independent variables on nanocarrier size*

3.3.2b Influence of independent parameters on encapsulation efficiency

The influence of various factors on encapsulation efficiency is shown in Figure 3.4 and Eq. 3.5 The obtained encapsulation efficiency ranges from 50.6% to 99.22%. Increasing the pH increases entrapment efficiency while increasing polymer to cross-linker ratio and reaction decreases time entrapment efficiency. Multiple linear regressions generate mathematical polynomial equations with constants and regression coefficients. Equation (2) can explain the effect of the independent parameter on entrapment efficiency;

$$Y2 = 100.33 + 28.50X_1 - 8.83X_2 - 52.83X_3 - 7.5X_1^2 + 4.5\,X_2^2 + 10.5X_3^2 \quad Eq.3.5$$

Regression equations depicted the relationship of the variables to the measured response. The pH has a positive impact on entrapment efficiency. The polymer-to-cross-linker ratio and reaction time inversely affect the entrapment efficiency. The higher the magnitude

of the coefficient, the higher the contribution of that factor toward the selected response. The higher values of the coefficient of pH represent its highest contribution towards the entrapment efficiency.

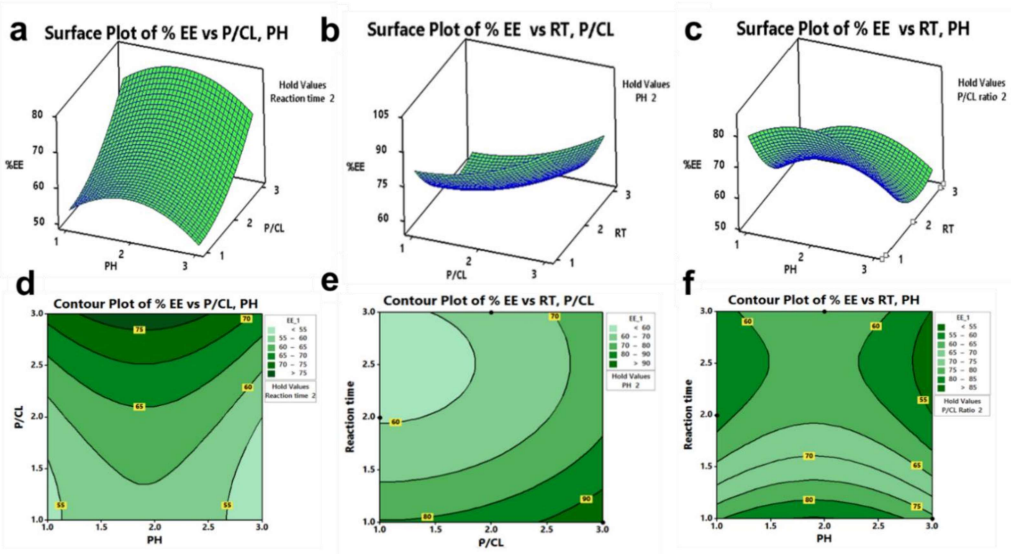

Figure 3.4: 3D response surface (a, b, & c) and their corresponding 2D contour plot (d, e, & f) showing mutual interaction and discrete effects of independent variables on % entrapment efficiency

3.3.2c Influence of independent parameters on drug loading

The influence of various factors on loading capacity is shown in Figure 3.5 and Eq 3.6. The obtained drug loading capacity ranges from 12 % to 56 %. Increasing the pH and polymer-to-cross-linker ratio decreases the loading capacity. While on increases the reaction time, the loading capacity was increased. Multiple linear regressions generate mathematical polynomial equations with constants and regression coefficients. Eq.3.6 can explain the effect of the independent parameter on entrapment efficiency

$$Y3 = -92.7 + 82X_1 + 164.67X_2 - 79.33X_3 - 18X_1^2 - 44X_2^2 + 20X_3^2 \qquad Eq.3.6$$

Regression equations depicted the relationship of the variables to the measured response. The pH and polymer-to-cross-linker ratio inversely affect the drug loading capacity. In contrast, the reaction time has a positive impact on the entrapment. The higher the magnitude of the coefficient, the higher the contribution of that factor toward the selected response. The higher magnitude of the polymer-to-cross-linker ratio coefficient represents its highest contribution toward the drug loading capacity.

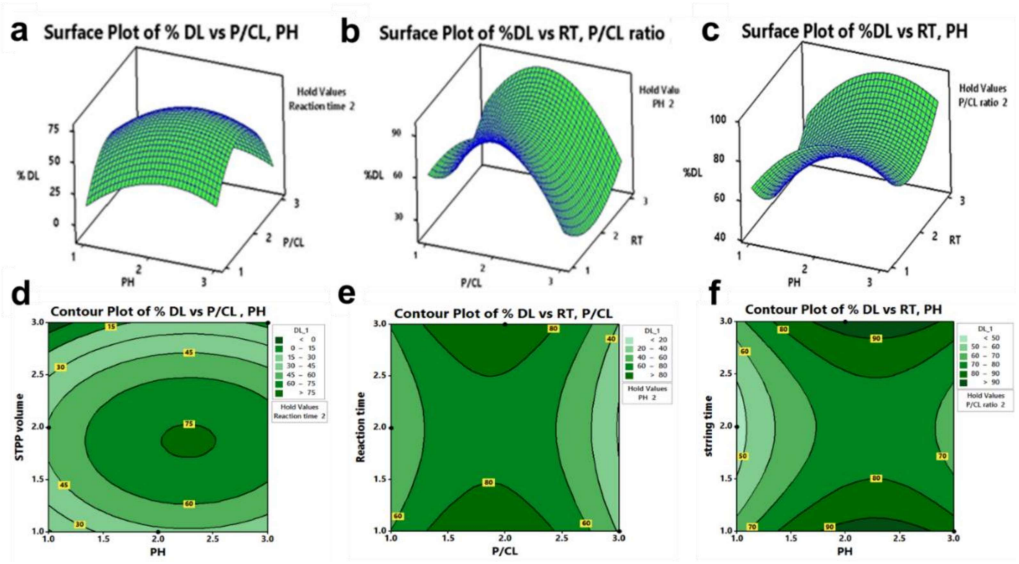

Figure 3.5: *3D response surface (a, b, & c) and their corresponding 2D contour plot (d, e, & f) show mutual interaction and discrete effects of independent variables on % drug loading.*

3.3.3 Optimization and checkpoint analysis (validation of predicted values)

Optimizing the independent variables by setting goals for each response and crea,ting an overlay graph global desirability function (D) was applied simultaneously to optimize the models obtained from experimental statistical analysis. All three independent variables were incorporated in the optimization of their design space. Each response had a low and high value assigned to each goal for concurrent optimization. The particle size response

was set to a minimum goal, while entrapment efficiency and drug loading capacity were adjusted to maximize. Thus, an individual desirability function (D) was proposed for each response whose values were expressed using a nondimensional scale ranging from 0 –1. Predicted responses were selected based on desirability factors. Criteria for optimal formulations were framed based on minimum nanocarrier size, maximum drug loading, and high entrapment efficiency.

DOE conducted the numerical optimization to identify the optimum combination of constraints, justifying the desired conditions. This optimization aimed to get the maximum response satisfying all variable properties simultaneously. The regression model developed in this study has been used to identify the optimal conditions to prepare nanoparticles with minimum size, maximum entrapment efficiency, and drug loading. The mean response refers to the average value of the performance characteristics for each parameter at a different level. The optimization plot of multiple responses is shown in Figure 3.6. Table 3.6 shows the optimal condition for the synthesis of M-CNCs. The composite desirability for M-CNCs is 0.7280.

The optimal formulation served as a checkpoint to validate the statistical method, and M-CNCs were synthesized using these optimal process variables. The percent errors were calculated according to values obtained for the responses and compared with estimated values. The predicted optimum conditions were applied experimentally to validate the models to improve the nanocarrier size, % EE, and % DL.

The experiment has been conducted based on the predicted values in triplicate. The optimized value for pH, polymer-to-cross-linker ratio, and reaction time was found to be 6.4, 10/3 mL, and 1 h, respectively. The predicted values for nanocarrier size, % EE, and % DL are 150 nm (d = 0.90838), 92.6 % (d = 0.87135), and 52.94 % (d = 0.48745), respectively. The % relative error was calculated using Eq.3.7.

$$Relative\ error\ (\%) = \frac{Predicted\ value - Practical\ value}{Practical\ value} \times 100 \qquad Eq.3.7$$

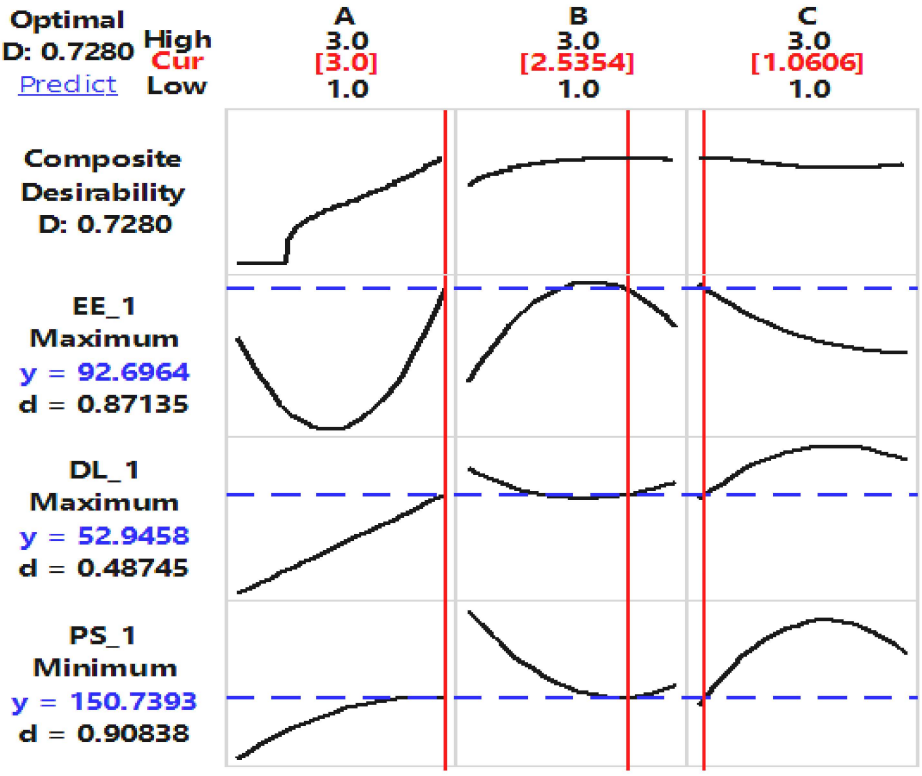

Figure 3.6: *Optimization plot of multiple responses*

Table 3.6. *Optimized formulation batch of Methotrexate-encapsulated chitosan nanocarrier with a predicted and experimental response with its relative error.*

Parameters	Goal	Lower limit	Upper limit	Optimized value	Predicted value	Experimental value	Relative error
pH of chitosan soulution (A)	Optimal	2.4	6.4	4.4	-	-	-
Polymer/cross-linker ratio (B)	Optimal	10/1	10/5	10/3	-	-	-
Reaction time (C)	Optimal	1	6	1	-	-	-
Particle size (Y_1)	Minimum	102	634	-	150	155	+5
Entrapment efficiency (Y_2)	Maximum	50%	99%	-	92 %	87%	- 5 %
Drug loading (Y_3)	Maximum	12%	96%	-	52.9%	49%	-3.94%

3.3.4 Physiochemical evaluation

3.3.4a Organoleptic evaluations

The optimized M-CNCs formulation was transparent, slightly yellowish, and free from any sign of precipitation, sedimentation, or aggregation, as shown in the inset figure (Figure 3.7a).

3.3.4b UV visible spectroscopy

The UV-vis absorbance spectra of placebo chitosan nanoparticles (Cs-NPs) did not show an absorbance peak of MTX. In contrast, M-CNCs have the MTX absorption peak at 303 nm, as shown in Figure 3.7a, indicating MTX's successful loading into the nanocarrier. The UV absorbance calibration curve for estimating MTX is shown in the inset figure

(Figure 4a). The linearity was found within 12 to 20 µg/mL with the regression equation Y= 0.0316 + 0.1308 (r^2= 0.986).

3.3.4c Fourier transform infrared spectroscopy

FTIR is extensively used to investigate the structure and analyze the functional groups. The FTIR spectra of MTX, chitosan, and M-CNCs are shown in Figure 3.7b. Free MTX shows a characteristic transmittance vibration peak, a broad band at 3371 cm^{-1} indicates N-H stretching vibrations, and a weak shoulder absorption at ~2944 cm^{-1} was attributed to symmetric and asymmetric CH_2 stretching vibrations, and the intense infrared absorption band at 1644 cm^{-1} was due to the carbonyl stretching vibration partially overlapped with the δ(N–H) band [211], while 1603 cm^{-1} and 1407 cm^{-1} correspond to the asymmetrical and symmetrical stretching vibrations of COO^- [212]**.** Chitosan shows characteristic vibrational peaks at 3447 cm^{-1} attributed to -OH group stretching vibration. The 1657 cm-1 and 1598 cm-1 peaks are attributed to the $CONH_2$ and NH_2 groups, respectively. These peaks shift to 1639 and 1557 cm^{-1} in the FTIR spectra of M-CNCs. This shift suggests the existence of ionic interaction between the NH^{3+} group of chitosan negatively charged MTX and phosphate groups of TPP [213], thereby proclaiming nanocarrier formation [214]. Another observation also clarifies this; the cross-linking with STPP was visible in the M-CNCs spectra, which showed bands at 1257 cm^{-1} and 1022 cm^{-1} that characterized the presence of P=O and aliphatic P-O-C groups.

3.3.4d X-ray diffraction

The XRD spectra of chitosan displayed sharp peaks at 2θ of ~ 20.4°. It represents a partially crystalline nature. The MTX showed several distinct, intense peaks at 2θ values of 9.48°, 11.1°, 12.8°, 14.5°, 16.4°, 19.7°, and 25.5°, representing its crystallinity. M-CNCs spectra also show crystalline nature with intense peaks at 2θ values

11.44°,17.01°,19.15°, 22.66°, 29.76°, 33.75°, and 36.66°, as shown in Figure 3.7c. Hence, the ionic gelation method and coupling of chitosan with MTX resulted in the formation of crystalline M-CNCs [215]. Therefore, the ionic gelation process and the coupling of chitosan with MTX led to the creation of crystalline M-CNCs.

3.3.4e Thermogravimetric analysis

TGA is a thermal technique that measures the changes in material mass as a function of temperature or time during heating in a controlled environment. It represents the material thermal stability and composition. The TGA data of M-CNCs demonstrates a four-step decomposition profile, as shown in Figure 3.7d. The M-CNCs showed a continuous 10 % weight loss from 33→166.5°C, 11.2 % weight loss from 166.5→268.7°C, 18.3% weight loss from 268.7→ 331.7°C, 11.8 % weight loss from 331.7 → 425.4 °C, and 10.1 % weight loss from 425 → 700 °C [216].

3.3.4f High-resolution transmission electron microscopy

High-resolution transmission electron microscopy (HR-TEM) shows the homogenous particle distribution in a system with a mean particle size of 35.7±9.1 nm (Figure 3.8).

3.3.4g Hydrodynamic size and zeta potential

All the formulations were within the size range from 102 nm to 634 nm. The particle size of less than 200 nm allows the passive tumor targeting via the EPR effect while avoiding reticuloendothelial system uptake [24]. The PDI value of the nanoparticle represents the homogeneity of particle size distribution. The values range from 0 to 1, whereas the PDI value of 0.1 to 0.25 represents a monodisperse sample with a narrow size distribution. In contrast, a PDI of more than 0.5 represents polydispersity and a broad distribution [217]. The PDI values of the formulations were found to be within the range of 0.37 to 0.9.

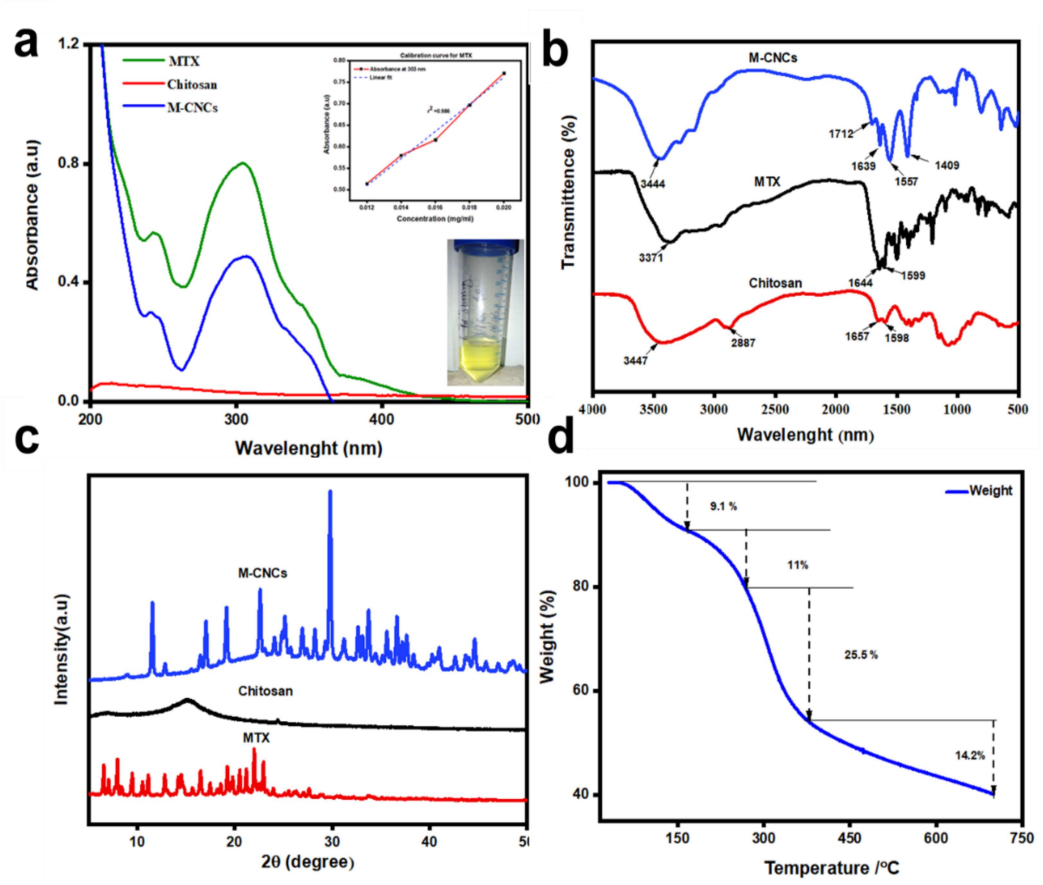

Figure 3.7: ***(a)*** *Absorbance spectra and inset figure show UV absorbance calibration curve of MTX,* ***(b)*** *FTIR spectra of chitosan, free MTX, and MTX-encapsulated chitosan nanocarrier (M-CNCs),* ***(c)*** *X-ray diffraction spectra for chitosan, free MTX, and M-CNCs, and* ***(d)*** *TGA curve of M-CNCs.*

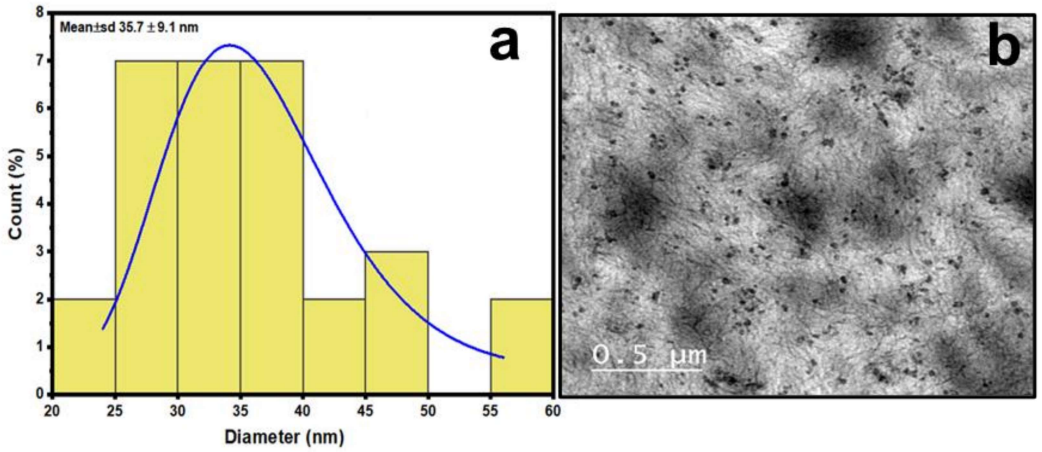

Figure 3.8: *a) Particle distribution curve using TEM image and b) HR-TEM image of Cs-NPs Nanoparticles*

The lower PDI value in most formulations reflects monodispersed and narrow size distribution. The lower PDI value will prevent the Ostwald ripening and offer stability. The ZP values are an indication of colloidal stability. Appropriate ZP is required for maintaining colloidal stability through the retention of sufficient repulsive force among colloidal particles. The ζ values mostly range from -30 to +30 mV, wherein the value from ± 0 to 10 mV indicates highly unstable, ± 10 to 20 mV shows relatively stable, and ±20–30 mV indicate moderately stable, and values higher than ± 30 mV are highly stable in nature of colloidal dispersion [218]. The larger the value of ZP more is the more dispersion stability. The ZP value of various batches was within the range of +1 to +34 mV (ZP) of M-CNCs signifies the high stability of the prepared formulations (Figure 3.9 & Table 3.7).

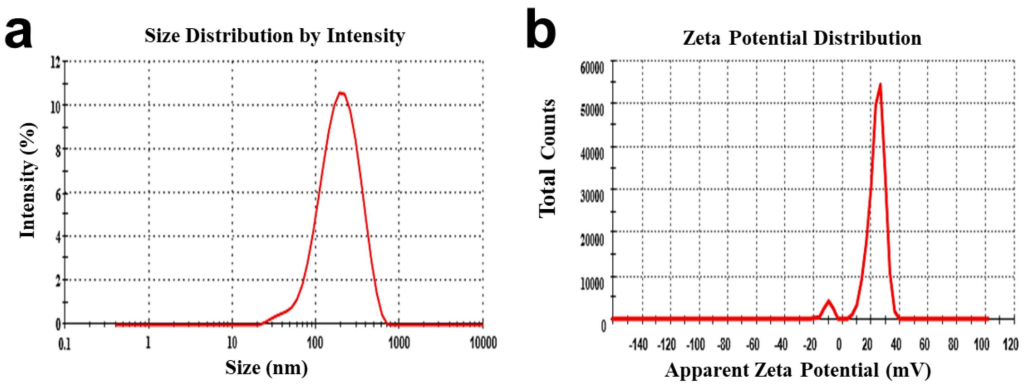

Figure 3.9: *Particles size and zeta potential graph of optimization nanocarrier*

3.3.4h Percent entrapment efficiency and drug loading

The entrapment efficiency of various formulations within 50 % to 99 % and the drug loading 12 % to 56 % was found (Table 3.2).

Table 3.7. *Nanocarrier size, PDI, and Zeta potential of M-CNCs*

Formulation	Runs	Nanocarrier size (nm) Z(av)	PDI	Zeta Potential (eV)
F1	1	160±1.7	0.6±0.05	+34±0.05
F2	2	186±16.6	0.37±0.05	+34.8±1.7
F3	3	200±27	0.67±0.46	+6.5±0.66
F4	4	634±15	0.6±0.17	+27.8±1.77
F5	5	224±13.9	0.44±0.02	+1.66±0.11
F6	6	102±29	0.74±0.29	-7±0.66
F7	7	494±36.4	0.59±0.07	+10.2±0.24
F8	8	216±6.08	0.44±0.02	+1±0
F9	9	352±11.9	0.9±0	-1±0

Values are expressed as Mean ± S.d; n=3

3.3.5 Storage stability

At the end of the stability study, the stability-indicating parameters were compared. The formulated M-CNCs were found to be a clear, homogeneous, transparent, yellowish-colored solution free from any gritty particles while accessed at the end of the long term. They accelerated the stability study (heating-cooling & freeze-thaw). The refractive index (RI) was found to be 1.331±0.001, close to the RI of water (1.33), reflecting the transparency and optical clarity of the formulation. The RI remained unaltered while evaluated at various time intervals and at the end of the study, representing the retention of homogeneity throughout the study. Further, the RI of samples taken from different regions of the same formulation was found to be the same (1.331 ± 0.001), representing the uniformity and isotropic nature of the M-CNC.

Studies were performed at two different temperatures at 4 ± 2ºC/ 60 ± 5% relative humidity (RH), at 40 ± 2ºC / 75 ± 5% RH for 90 days, with 30 days intervals. The long-term storage stability of the drug-polymer nanoparticles is an essential prerequisite.

Nanoparticle formulations increase the surface area by many folds, leading to very high aggregation after long storage periods. Table 3.8 represents the effect of storage time on particle size, zeta potential (ZP), polydispersive index (PDI), and % entrapment efficiency (% EE) of M-CNCs.

From Table 3.8, at 4°C, the results show that up to 60 days, no change in M-CNCs size was discernable. While, beyond 60 days, M-CNCs size increased slightly (155 to163 nm). The nanoparticles appeared to be stable without any collapse or aggregation. At the same time, formulations stored at 40°C were observed to have no change in size up to 60 days. However, beyond 60 days, M-CNCs were slightly larger (155 to 162 nm) than the original size (Figure 3.10a). It could be due to the slight aggregation of particles in the formulation. There were no significant changes in nanoparticles besides a slight increase in particle size and a slight decrease in encapsulation efficiency. Due to aggregation, the particle size distribution curve tends to become non-Gaussian.

The PDI value of the nanoparticle represents the homogeneity of particle size distribution. The PDI values at various time points at two different storage conditions were within 0.26 ± 0.001 to 0.30 ± 0.002 (Figure 3.10b), below the borderline (0.5) of polydispersity, indicating particle size homogeneity.

A slight decrease in zeta potential (34 ± 0.37 to 32 ± 0.39 mV) as a function of an increase in storage time was noticed after 90 days. Still, the presence of a very high positive charge (32 ± 0.39 mV) on the surface of the nanoparticles is sufficient to maintain the repulsive force among them, which will prevent them from aggregation and keep the stability of the M-CNCs (Figure 3.10c). The entrapment efficiency was slightly decreased from 87 ± 0.1 % to 85.1 ± 0.1 % over the 90 days of storage (Figure 3.10d).

Table 3.8. *Long-term Storage stability of M-CNCs at 4℃ and 40℃*

Long-term stability study						
		4℃				
Storage time (days)	**Organoleptic properties**	**RI**	**Nanocarrier size (nm)**	**Zeta potential**	**PDI**	**EE (%)**
0 day	Clear, Transparent, Yellowish colored, Homogeneous	1.333	155±0.22	34±0.44	0.26±0.001	87±0.1
30 days		1.333	155±0.24	34±0.38	0.26±0.002	87±0.09
60 days		1.335	159±0.21	33.2±0.39	0.27±0.0011	86±0.1
90 days		1.335	163±0.24	30±0.42	0.29±0.002	85.1±0.1
		40℃				
0 day	Clear, Transparent, Yellowish colored, Homogeneous	1.333	155±0.24	34±0.37	0.26±0.0017	87±0.10
30 days		1.333	155±0.17	34±0.38	0.26±0.002	87±0.08
60 days		1.334	160 ±0.22	33.2±0.40	0.28±0.0029	86.4±0.1
90 days		1.334	162±0.18	32±0.39	0.30±0.002	85.5±0.11
		Accelerated stability study				
		After Heating-cooling cycle				
0 day	Clear, Transparent, Yellowish colored, Homogeneous	1.333	155±0.24	34±0.44	0.26±0.001	87±0.1
30 days		1.334	155±0.24	34±0.44	0.26±0.001	87±0.1
60 days		1.334	162±0.44	32±0.49	0.39±0.001	86.9±0.1
90 days		1.335	167±0.64	30±0.55	0.42±0.001	85.1±0.1
		After Freeze-thaw cycle				
0 day	Clear, Transparent, Yellowish colored, Homogeneous	1.333	155±0.24	34±0.44	0.26±0.001	87±0.1
30 days		1.333	155±0.24	34±0.44	0.26±0.001	87±0.1
60 days		1.333	155±0.24	34±0.44	0.31±0.0011	86.2±0.1
90 days		1.333	160±0.24	33±0.23	0.33±0.0011	85.7±0.1

RI=Refractive Index, [b] PDI=Polydispersive Index, % EE = Percent Entrapment Efficiency. Results are expressed as the mean ± standard deviation (S.d) (n=3).

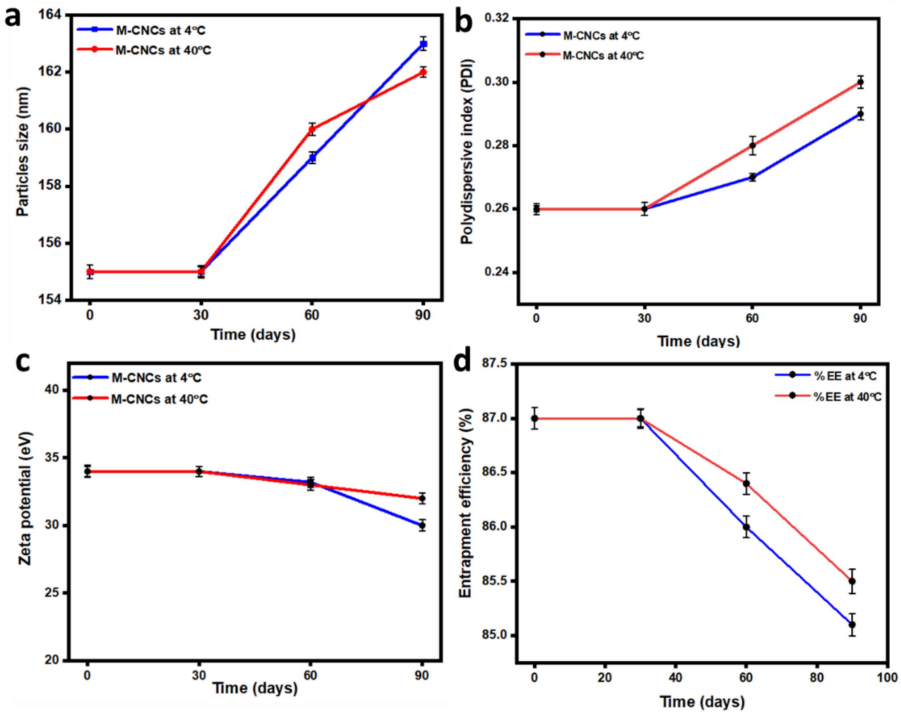

Figure 3.10: ***(a)*** *Particles size,* ***(b)*** *PDI,* ***(c)*** *Zeta potential,* ***(d)*** *% Entrapment efficiency displays stability studies of nanoparticles at 4 ± 2ºC/ 60 ± 5 % (RH) and 40 ± 2ºC / 75 ± 5 % RH.*

The slight decrease in the % EE might be due to the leakage of the drug from the nanocarrier over time. Overall, the stability study results indicate the vast storage potential of the prepared M-CNCs without any significant degradation or loss of colloidal nature.

3.3.6 *In-vitro* drug release and kinetic model and Mechanism

The release of MTX from the nanocarrier and unformulated free MTX has been carried out using a dialysis membrane at pH 6.4 and 7.4 in phosphate buffer solutions (PBS). The cumulative percentage of drug release was plotted against time to obtain the drug release profile. When we looked at the cumulative percent release of free MTX after 72 hours, we found that it was ~28% at pH 6.4 and ~57% at pH 7.4, respectively. The release of

free MTX was faster than that of MTX-encapsulated nanocarriers, although only 7% at pH 6.4 and 30% at pH 7.4, respectively. At pH 6.4, MTX releases four times more slowly from nanocarriers than free MTX, whereas at pH 7.4 is around two times slower. The side effects of a drug may be diminished by controlling the release of the drug. Because the polymer matrix is a barrier between the drug and the solvent medium, the drug is released slowly, resulting in controlled release (Figure 3.11).

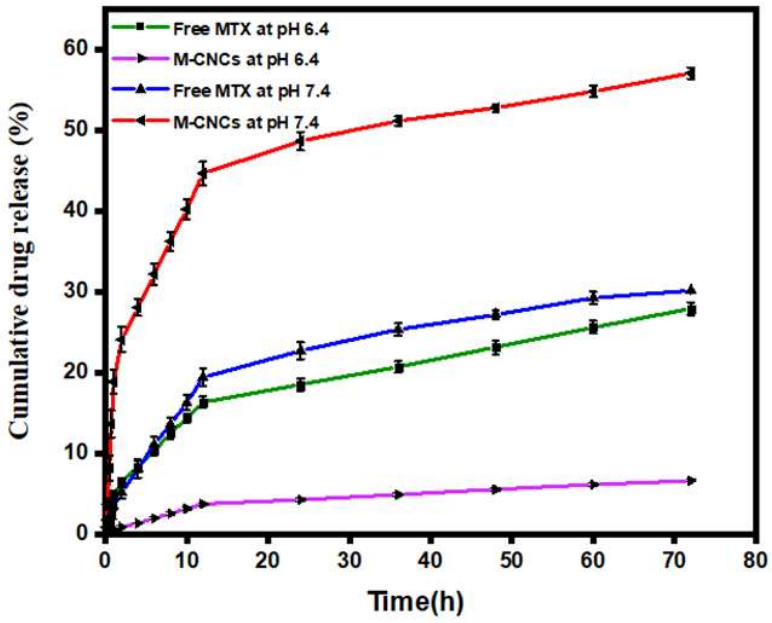

Figure 3.11: *in-vitro drug release studies at two different pH, Results are expressed as the mean ± S.d (n=3).*

The kinetic model is often helpful in elucidating release mechanisms. The data from *in-vitro* drug release studies were plotted to conduct the kinetic model. The *in-vitro* drug release data were then fitted to different kinetic models, including the zero order, first order, Higuchi model, and Korsmeyer-Peppas model. The best-fit kinetic model was thought to be one where the regression coefficient was near unity. The kinetic model coefficient was calculated using regression analysis (Table 3.9). Additionally, to understand the drug release mechanism, the data were fit using the Korsmeyer-Peppas

model, $\frac{Mt}{M\infty} = Kt^n$ where the exponent '*n*' value represented the drug transport method. The mechanism of diffusion can be evaluated using the n value. The kinetics of the drug release mechanism at pH 6.4 for free MTX and MTX-encapsulated nanocarrier with R^2 values of 0.965 and 0.977, respectively. While at pH 7.4, R^2 values were 0.977 and 0.955, respectively (Table 3.9). Drug release follows the Higuchi kinetic model. The diffusion and swelling process control the drug release. When the polymer system comes into contact with the solvent, the rearrangement of the polymeric chain starts slowly with the diffusion process simultaneously [219].

Table 3.9. *In-vitro drug release kinetic models fit for free MTX and M-CNCs with the regression coefficient*

Kinetic models	**Rate Equations**	**Free MTX (pH 6.4) R^2**	**Free MTX (pH 7.4) R^2**	**M-CNCs (pH 6.4) R^2**	**M-CNCs (pH 7.4) R^2**
Zero-order	$Q_t = Q_0 + K_0 t$	0.814	0.99	0.882	0.806
First order	$\log C = \log C_0 - \frac{Kt}{2.303}$	0.913	0.958	0.958	0.945
Higuchi *	$Q = K_H t^{1/2}$	0.965	0.977	0.977	0.955
Korsmeyer-Peppas	$\frac{Mt}{M\infty} = Kt^n$	0.941	0.964	0.964	0.949

R^2 = Regression coefficient , Best fitted model*

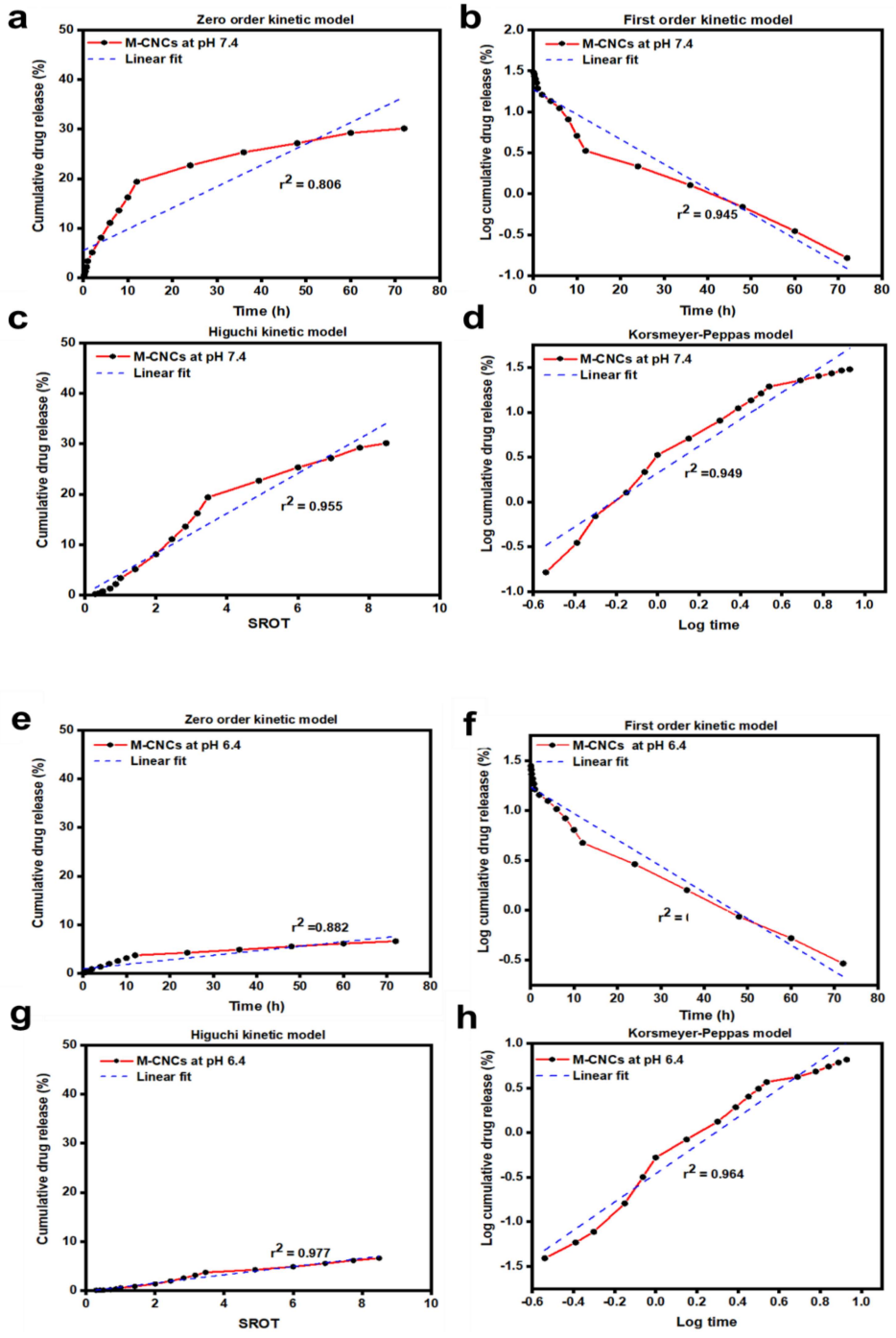

Figure 3.12: *In-vitro drug release data fit into kinetic models; zero order, first order, Higuchi models, and Korsmeyer-Peppas;* ***a,b, c****, and* ***d*** *at pH 6.4, whereas* ***e,f, g,*** *and* ***h*** *at pH7.4*

3.4 Animal studies

3.4.1 *In-vivo* pharmacokinetics

The time-dependent plasma drug concentrations of free MTX and M-CNCs in Sprague Dawley rats are shown in Figure 3.13, and the pharmacokinetic parameters are summarized in Table 3.10. From Table 3.10, results show that the nanoparticle increases the elimination half-life ($t_{1/2}$), nearly 1.5 times higher than the free MTX. The increased half-life will allow more extended circulation of MTX in the systemic circulation and prolonged therapeutic activity. In the area under the curve (AUC_{total}), the total systemic exposure to the drug was increased three times compared to the free MTX, representing the improvement of bioavailability. MTX's clearance rate (CL) in the form of M-CNCs was 1.5 times slower than the free MTX.

Table 3.10. *Pharmacokinetic parameter of free MTX and M-CNCs in plasma of rats after intravenous administration of the equivalent dose of 5 mg/kg of MTX*

Pharmacokinetic parameters	**Free Methotrexate**	**M-CNCs**
AUC_{total} (µg/ml×h)	0.117	0.145
C_{max} (µg/ml)	0.875	2.294
T_{max} (h)	0.25	0.5
Vd (ml)	2356	1966
$t_{1/2}$ (h)	38.4	49.6
CL (µl/h)	42426	27477

AUC_{total} = area under the curve, C_{max} = maximum concentration, T_{max} = maximum time, Vd = volume of distribution, $t_{1/2}$ = elimination half-life, and CL= clearance rate. Results are expressed as the mean ± S.d (n=3).

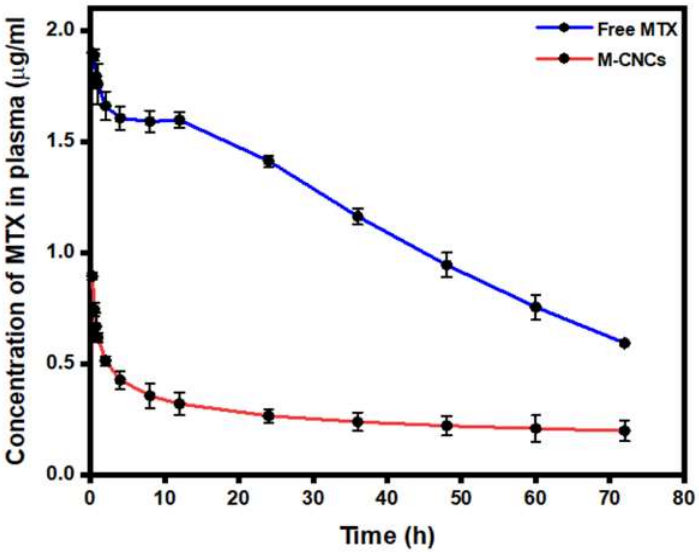

Figure 3.13: *Concentration–time profiles of MTX in blood plasma after iv administration of free MTX and M-CNCs. Results are expressed as the mean ± S.d (n=3).*

3.4.2 Histopathological studies

The transverse sections of the liver and kidney from the rats in the control and nanoparticle-treated group after microscopic analysis are depicted in Figure 3.14. Comparing the vital organs of animals treated with M-CNCs nanoparticles with the control group, a macroscopic examination of the treated animal organs showed no differences in morphology and texture. The histopathological examination of the rats from the control group and those treated with nanoparticles revealed normal organ architecture and the absence of any noticeable pathological changes or lesions, representing the safety of the prepared M-CNCs.

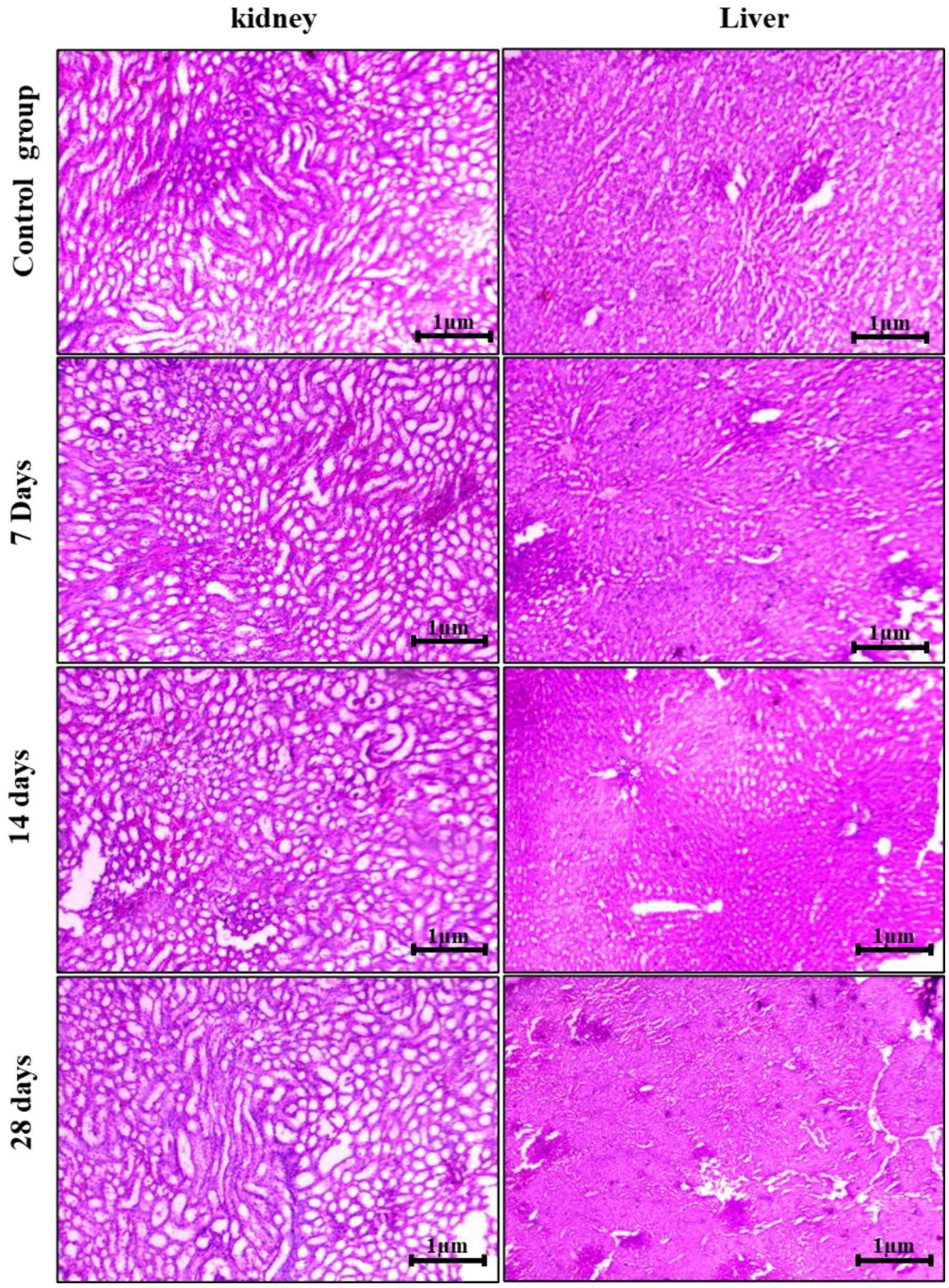

Figure 3.14: *Histopathological of the kidney and liver of the rats comparing the control group and those treated with M-CNCs at 7, 14, and 28 days revealed normal organ architecture and the absence of any noticeable tissue lesions.*